Progress In Electromagnetics Research M, Vol. 112, 177–189, 2022

Design of a Wideband Spring Textile Antenna for Wearable 5G and IoT Applications Using Characteristic Mode Analysis

Bashar Bahaa Qas Elias[1, *] and Ping Jack Soh[2]

Abstract—This paper presents the design and practical implementation of a wideband spring textile (WST) antenna for wearable communications. The antenna is designed on a felt substrate having a compact dimension of $32 \times 42 \times 3\,\text{mm}^3$ ($0.38\lambda_g \times 0.5\lambda_g \times 0.036\lambda_g$). This antenna operates in the 3.14 to 5.45 GHz frequency range, has a bandwidth (BW) of around 2306 MHz, and has a peak realized gain of 6 dBi at 3.5 GHz. Due to a broad frequency coverage, this antenna can be used in a wide range of wireless applications, including 5G and IoT. The proposed design is analyzed in terms of reflection coefficient, radiation pattern, efficiency, gain, and surface current. Using the same electromagnetic simulation software, both characteristic mode analysis (CMA) and the method of moments (MoM) are applied in the design process. The simulated results on a human chest phantom demonstrate the −10-dB impedance bandwidths of 1461 MHz. The antenna prototype is fabricated for verification, and the simulated and measured results demonstrate that the proposed antenna is suitable for wideband on-body applications given its low-profile implementation and mechanical flexibility.

1. INTRODUCTION

The study of body-centric communication systems is becoming one of the most researched topics worldwide [1]. To support communications in body area network (BAN) systems, flexible wearable antennas are being developed in facilitating data transfer between on-body devices and off-body nodes [2]. These wearable antennas are required to collect health data from patients to transmit data with more capacity using multiple 5G carrier bands [3]. Planar antennas are one of the essential antenna types that match these requirements due to their low cost, ease of fabrication, and small size [4]. Several factors must be considered to achieve the appropriate performance characteristics; for example, suitable bandwidth can be achieved by a wideband design [5]. Textile-based wearable systems are gaining popularity due to their prospective applications, which include navigation, tracking, health monitoring, and public safety [6].

The characteristic mode analysis (CMA) has been found to be a suitable method for designing antenna structures. CMA theory was first introduced in [7], and it has since been developed in [8, 9]. Its properties, which include the modal significance (MS), eigenvalue (λn), and characteristic angle (βn), allow it to visualize modes and individual current flows. CMA can provide a set of orthogonal currents characteristics, whose modes are numerically obtained for conductive bodies. These modes are only related to the antenna's structure, size, and frequency of operation. This allows CMA to provide physical insights of antenna radiation, increasing comprehension of the structure for efficient antenna design, synthesis, and optimization [10, 11].

This paper presents a compact and wideband spring textile (WST) antenna for wearable applications. The antenna operates with more than 2306 MHz of bandwidth, ranging from 3.14 to

Received 29 June 2022, Accepted 26 July 2022, Scheduled 4 August 2022
* Corresponding author: Bashar Bahaa Qas Elias (bashar.bahaa@sadiq.edu.iq).
[1] Department of Communications Technology Engineering, College of Information Technology, Imam Ja'afar Al-Sadiq University, Baghdad, Iraq. [2] Centre for Wireless Communications (CWC), University of Oulu, P. O. Box 4500, 90014 Oulu, Finland.

5.45 GHz. Its bandwidth enables operation of most of the current and prospective 5G frequency bands under consideration. Commercial electromagnetic simulator FEKO is used in design and simulation process which are done both using CMA and the method of moments (MoM). The designed antenna is prototyped and experimentally validated. Finally, the performance of the WST antenna is further examined near a body simulating phantom.

The paper is organized as follows. A detailed description of the WST antenna is first presented in the next section, followed by the operating mechanism of the antenna in Section 3. The simulated performance of the antenna in free space will be then analysed in Section 4 prior to the on-body evaluation and discussion in Section 5. Finally, Section 6 summarizes this paper with a conclusion.

2. DESIGN AND CONFIGURATION

Figure 1 shows the the proposed WST antenna designed on a felt textile substrate with a thickness (h) of 3 mm, dielectric constant of approximately 1.3, and loss tangent of 0.044. The single layered substrate ensures a low-profile structure and reduces potential complexities in fabrication and integration with clothing. The top patch and partial bottom ground are made using a ShieldIt conductive fabric. The overall antenna is fed by a microstrip feed line, with its width (Wf) optimized to ensure good impedance matching. The WST antenna has been simulated in FEKO simulator software for the 2.5 to 6 GHz frequency range, and different antenna parameters have been analyzed.

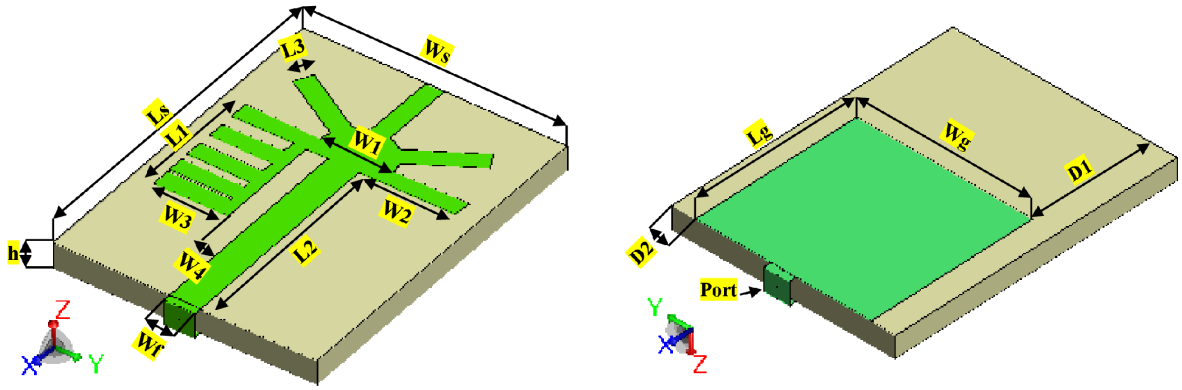

Figure 1. Configuration of the WST textile antenna. (a) Front view, (b) back view. $Ls = 42$ mm, $Ws = 32$ mm, $L1 = 15.3$ mm, $L2 = 26.625$ mm, $L3 = 2.25$ mm, $W1 = 8.97$ mm, $W2 = 11.625$ mm, $W3 = 9$ mm, $W4 = 2.625$ mm, $Wf = 3.75$ mm, $h = 3$ mm, $Lg = 24$ mm, $Wg = 25$ mm, $D1 = 18$ mm, and $D2 = 3.5$ mm.

3. FABRICATION PROCESS

The fabrication process of the antenna can be summarized as follows: i) The structure of the spring patch with the exact actual dimensions is printed on paper to prevent the patch from deforming or shifting during the subsequent patch-substrate integration process, as depicted in Fig. 2(a). ii) This paper is tightly secured on a piece of Shieldit fabric which is sized slightly larger than the patch size (see Fig. 2(b)). iii) The structures of the patch and ground planes are carefully drilled on the fabric using scissors and a blade, as shown in Fig. 2(c). iv) These planes are secured on the front and back sides of a piece of felt substrate, and a Sub Miniature Version A (SMA) connecter is soldered with the feed line using the silver epoxy, as illustrated in Fig. 2(d).

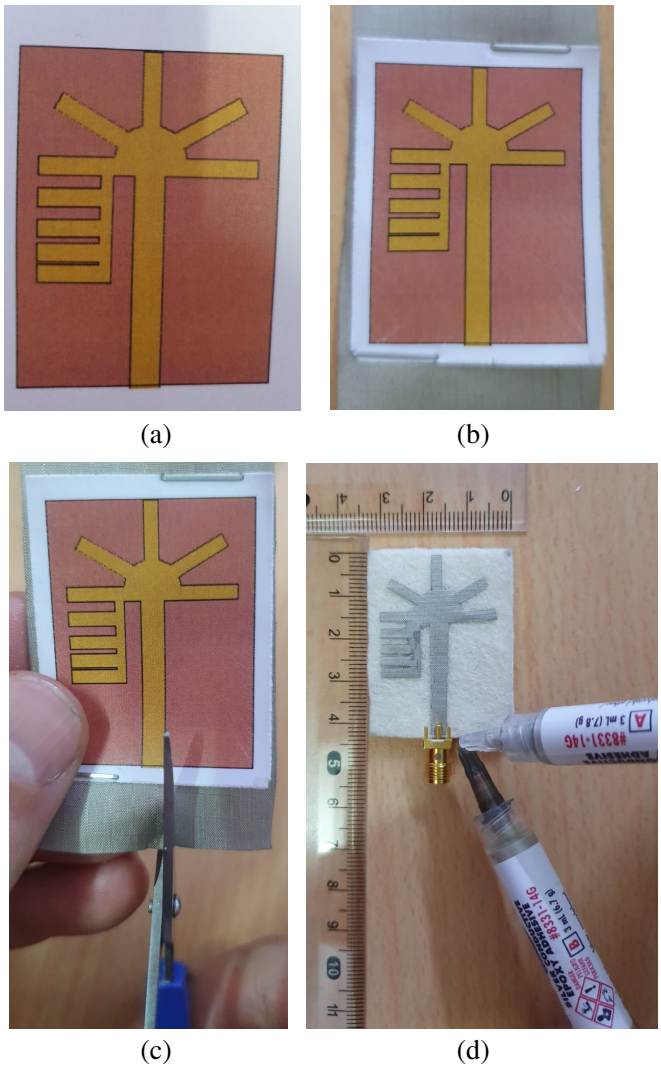

Figure 2. Antenna fabrication process (a) step 1, (b) step 2, (c) step 3, (d) step 4.

4. PERFORMANCE IN FREE SPACE

The antenna performance is simulated using FEKO software using two different methods, CMA and MoM. The design is optimized step by step prior to fabrication and measurements. The reflection coefficient of the proposed antenna is measured by a vector network analyzer (Anritsu model S362E) between 2.5 GHz and 6 GHz. Computations using FEKO software are performed on a computer with Intel (R) Core (TM) i5-2450 M 2.50 GHz CPU with 8.0 GB DDR3 RAM.

4.1. CMA Analysis

Results of modal significance (MS) are obtained using CMA in FEKO software during the design of the proposed antenna. MS is ranged between $0 < \text{MS} \leq 1$. The design steps of the antenna are performed in five steps, as shown in Fig. 3.

The simulation process using CMA includes only the radiating patch as a perfect electrical conductor without the substrate, ground, and excitation. The MS of the first design step is depicted in Fig. 4(a). It can be observed that the maximum value of MS of the first mode is achieved at approximately the target frequency of 3.5 GHz. In contrast, its value at the other bands for the first three generated modes is less than 0.7 (from 2.5 GHz to 3.1 GHz and from 4.1 GHz to 6 GHz), as

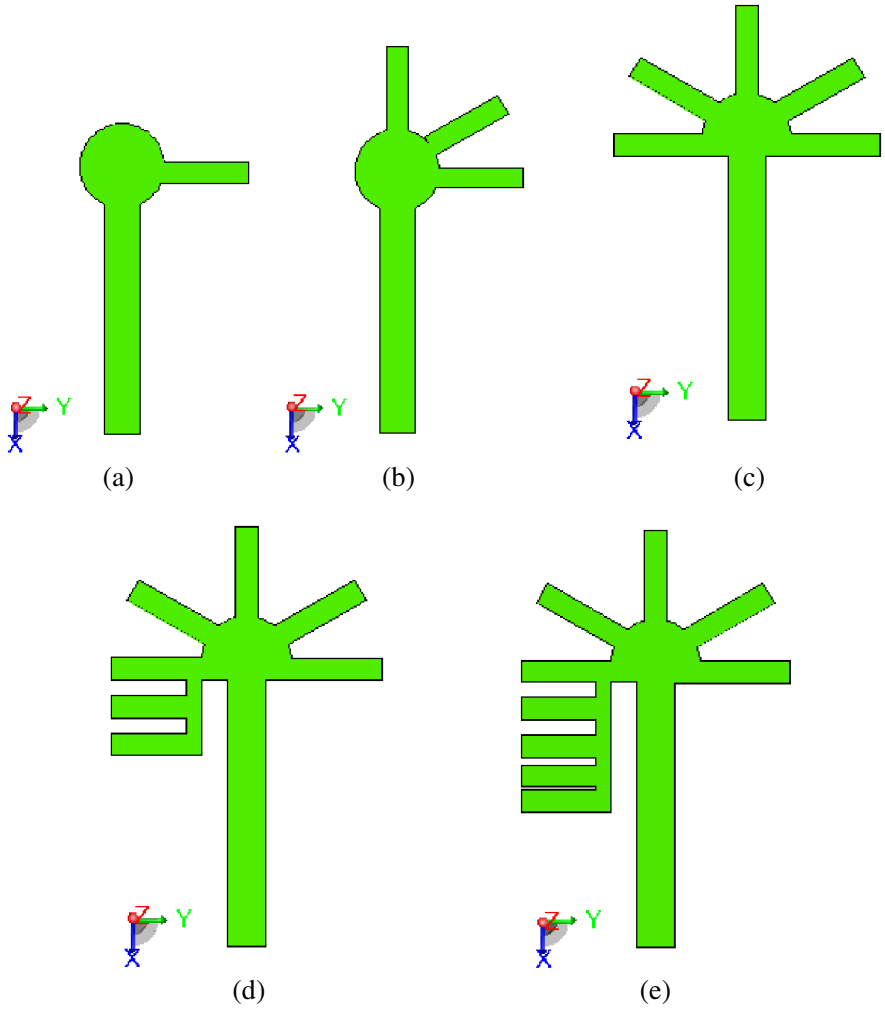

Figure 3. Design procedure of the WST antenna (a) step 1, (b) step 2, (c) step 3, (d) step 4, (e) step 5.

indicated by the black dashed line. In the second modification, two additional arms are added to the initial structure, as shown in Fig. 3(b). It is observed that mode 1 is still active at the target resonant frequency, and mode 2 starts shifting below 6 GHz (see Fig. 4(b)). After that, two more arms on the opposite site of the existing arms are added (Fig. 3(b)). As a result, both modes 2 and 3 cover the band from 4.25 GHz to 6 GHz, whereas at 3.5 GHz, the three modes show MS of less than 0.7, as illustrated in Fig. 4(c). This structure is further modified by adding another two more fingers, as

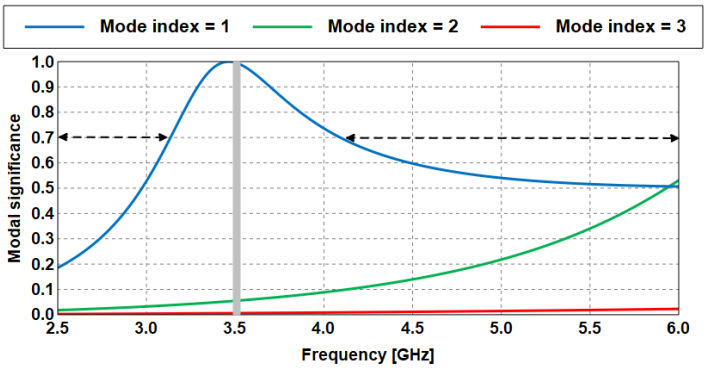

(a)

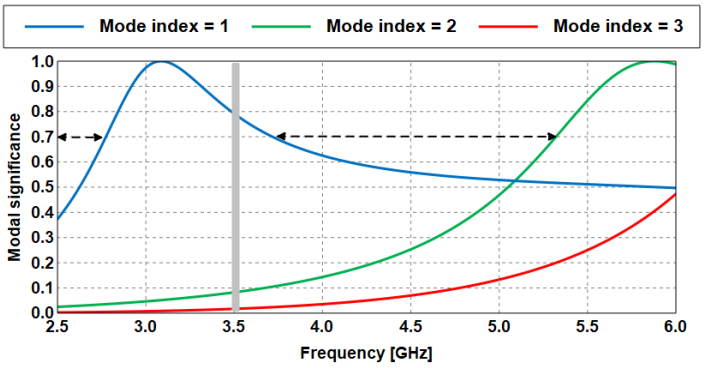

(b)

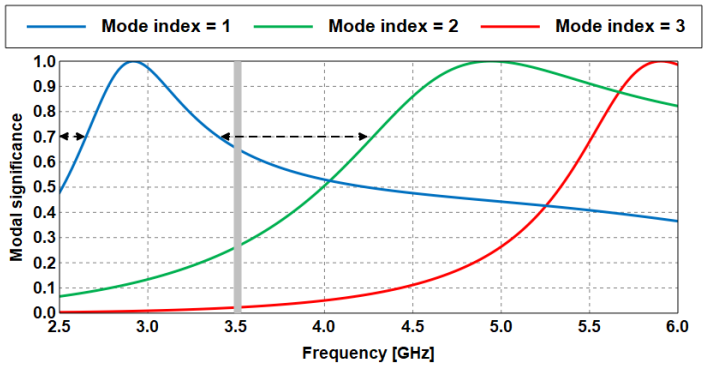

(c)

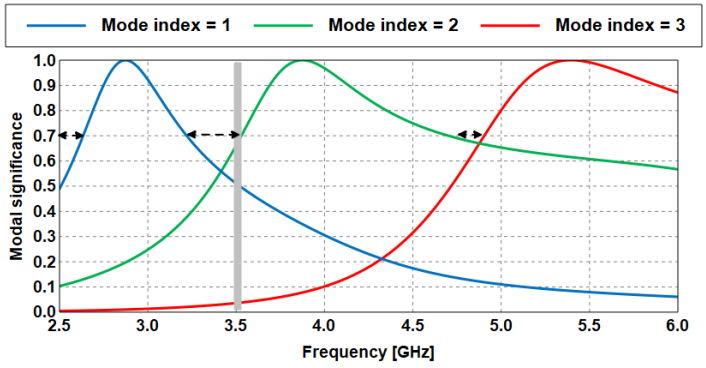

(d)

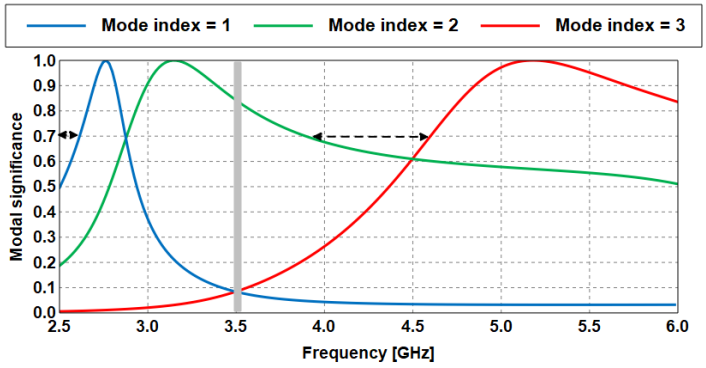

(e)

Figure 4. MS results at different steps of WST antenna (a) step 1, (b) step 2, (c) step 3, (d) step 4, (e) step 5.

depicted in Fig. 3(d). As observed in Fig. 4(d), the impedance bandwidth of the modes is increased by these additional elements. However, the MS value at 3.5 GHz remains less than 0.7. Finally, in step 5, another two more fingers as shown in Fig. 3(e) result in a high bandwidth within the frequency band of interest, as shown in Fig. 4(e). In short, CMA has facilitated the understanding of the structure and its behaviour.

4.2. MOM Analysis

As aforementioned, the additional spring elements can significantly widen the antenna impedance bandwidth without the need of increasing its substrate thickness. These elements can generate another resonant frequency, combined with the fundamental resonant frequency of the spring radiator, which produces enhanced impedance bandwidth. The antenna reflection coefficients obtained from simulations and measurements are satisfactory and are depicted in Fig. 5. Its operation frequency is extended from 2.99 GHz to 5.57 GHz with a fractional bandwidth of 73.8%. In simulations, this band indicates operation from 3.14 GHz to 5.45 GHz, with a fractional bandwidth of 66%. Compared to simulations, variations in measurement results originate from differences in material properties in practice and unavoidable movements due to the flexibility of the structure. Nonetheless, the antenna has operated successfully in the targeted operating bands.

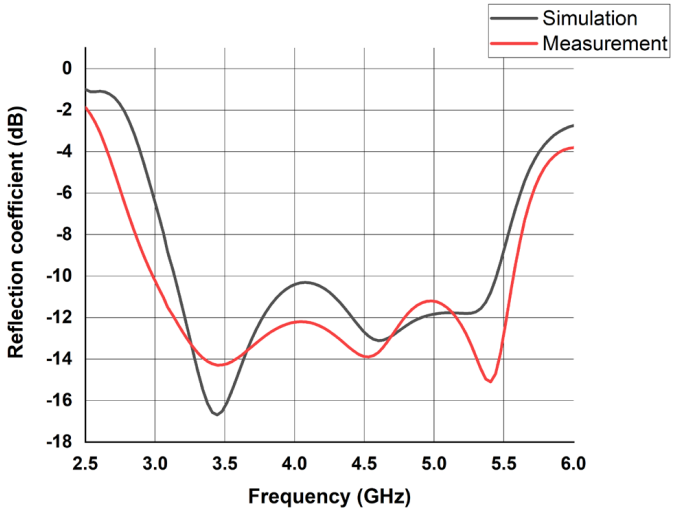

Figure 5. Simulated and measured reflection coefficients.

The simulated radiation patterns at 3.5 GHz and 4.8 GHz in the xz-plane and yz-plane are illustrated in Fig. 6. In the xz-plane, a typical gain distribution as a function of the vertical axis is observed, with a null in the direction of the horizontal axis at 3.5 GHz and 4.8 GHz. On the other hand, the patterns in the yz-plane show an omnidirectional characteristic at 3.5 GHz, whereas the direction of its maximum is closer to the horizontal axis at 4.8 GHz. The diffractions in patterns are due to the effect of the partial ground plane.

The current distribution in Fig. 7 indicates a noticeable current along the surface of the feed strip, in the semicircular element in the centre of the patch, and along the integrated vertical strip with the left side spring elements. The changing direction of the current path at different phases (0°, 90°, 180°, and 270°) is also observed.

Figures 8(a)–(b) show that the 3D radiation patterns are shown at 3.5 GHz and 4.8 GHz indicating a gain of 6 dB and 3.6 dB, respectively. At 3.5 GHz, the radiated power is distributed highly on the right side of the antenna. On the other hand, the radiation pattern is more intensively directed at the lower side of the antenna and is suppressed in the upper one.

Furthermore, the linear scale plot in Fig. 9 shows that the radiation efficiency varies from 87% to 62.8%, depending on the operating frequency (between 3 and 6 GHz).

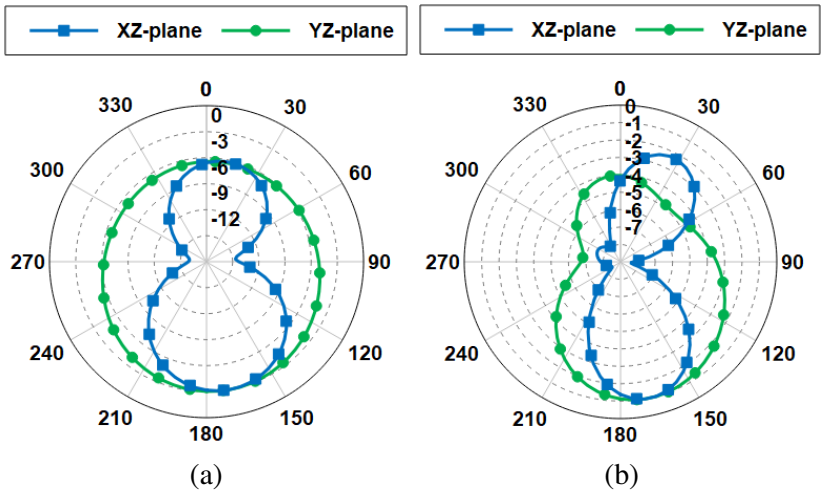

Figure 6. The normalized radiation patterns of the WST antenna in the xz-plane and yz-plane (a) at 3.5 GHz, (b) at 4.8 GHz.

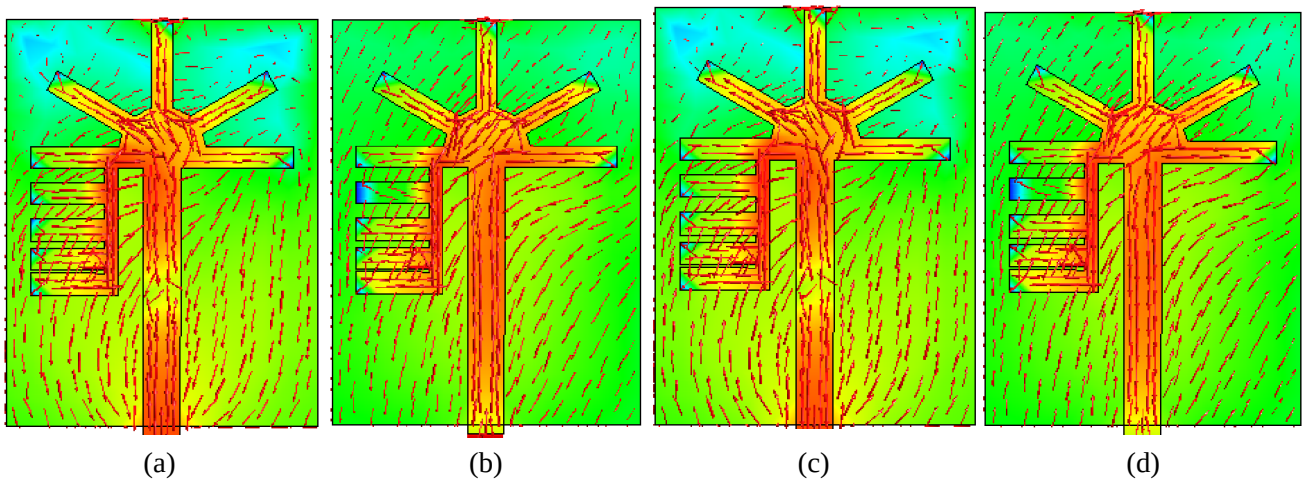

Figure 7. Simulated current surface distribution with different phases (a) 0°, (b) 90°, (c) 180°, (d) 270° at 3.5 GHz.

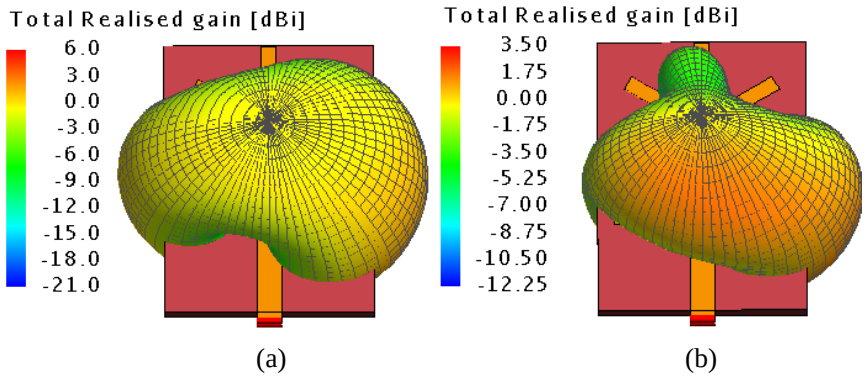

Figure 8. 3D far-field pattern with realised gain results of WST antenna (a) at 3.5 GHz, (b) at 4.8 GHz.

Optimal width values for each spring element have been chosen to operate with the required bandwidth while a compact size is maintained. Upon obtaining operation at a required resonant frequency, the width value of each spring element is optimized further, one at a time, using the genetic algorithm (GA) method [12] (see Fig. 10). The basic approach in GA for optimizing a primary square microstrip patch antenna is to divide the structure symmetrically into grids and then remove the smaller metallic grid squares from the patch. It is aimed at optimizing the reflection coefficient, with the results at different optimization run numbers (n) presented in Fig. 11 and Fig. 12.

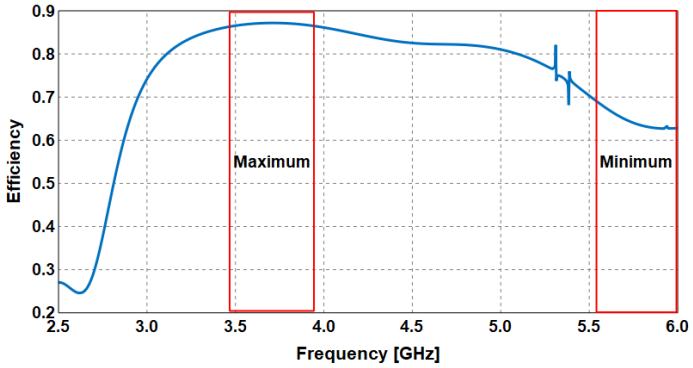

Figure 9. Efficiency results of WST antenna.

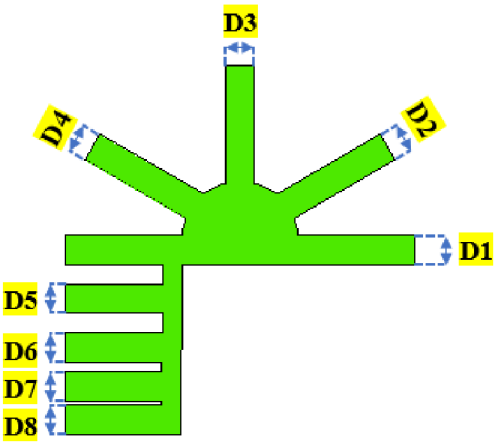

Figure 10. WST parameters that are optimized.

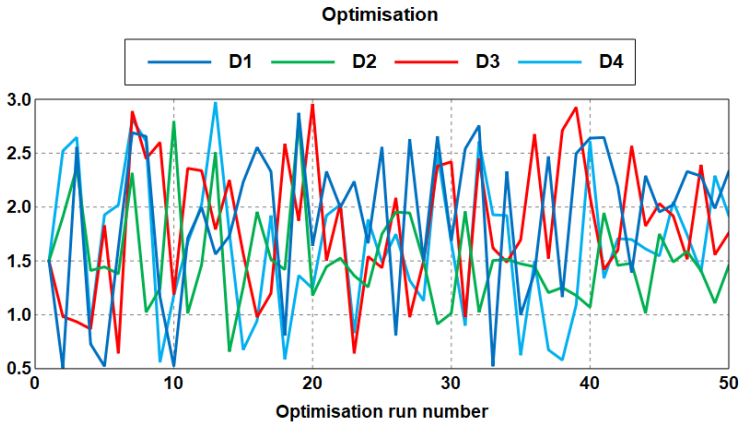

Figure 11. Results of optimization (D1–D4).

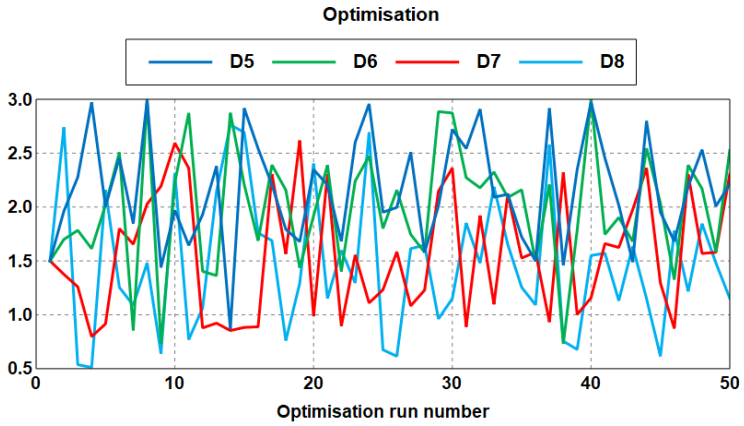

Figure 12. Results of optimization (D5–D8).

5. PERFORMANCE ON BODY

The antenna is then evaluated on body. In simulations, a heterogeneous model representing a human body is used. It consists of different layers: skin, fat, muscle, and bone, with different thicknesses, 1.6, 8, 10, and 5.4 mm, respectively, as depicted in Fig. 13 [13–15]. For experimental assessments, the antenna is placed on the chest of a human volunteer with a height and weight of 185 cm/97 kg, as shown in Fig. 14. The gap between the antenna and rectangular human tissue model or subject is kept at 5 mm, considering the thickness of cloth on the human body. The antenna may be deformed when being placed on a human body due to the different curvatures of the human body [16].

In simulations, the proposed antenna on the phantom body operated from 2.79 to 4.25 GHz with a bandwidth of 1461 MHz. At 3 and 3.5 GHz, the reflection coefficients are −17.04 dB and −13.8 dB, respectively, with realized gains of −5.3 dB and −7.5 dB (see Fig. 15). Meanwhile, the on-body

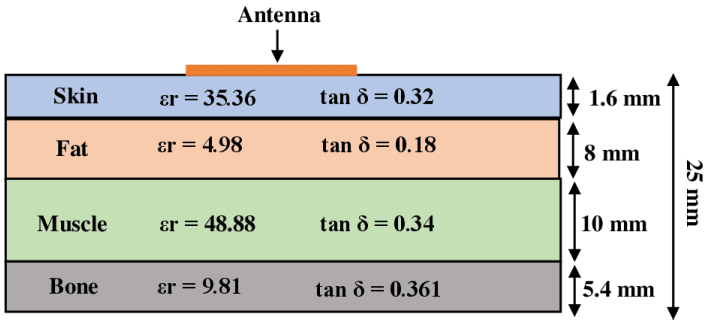

Figure 13. Side view of the heterogeneous model.

(a) (b)

Figure 14. (a) Antenna on phantom body, (b) antenna mounted on human body.

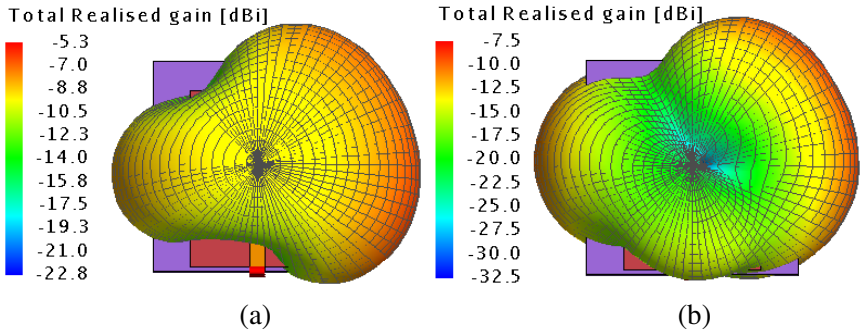

Figure 15. 3D far-field pattern with realised gain results of WST antenna on body (a) at 3 GHz, (b) at 3.5 GHz.

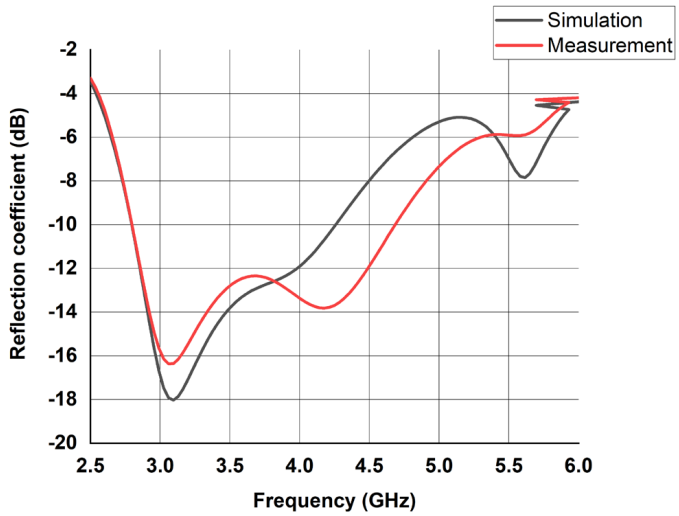

Figure 16. Reflection coefficient results on body.

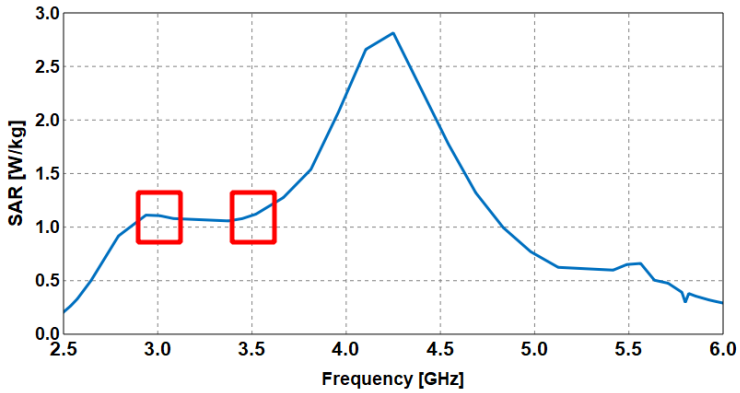

Figure 17. Side view of the heterogeneous model.

measurement results indicate a frequency range of 2.803 to 4.688 GHz, with a bandwidth of 1886 MHz. Simulated and measured reflection coefficients are compared in Fig. 16. Notably, the antenna gain deteriorated compared to free space due to the absorption by the human tissue. Table 1 compares simulated and measured results in free space and on-body.

Table 1. Simulated results in free space and on body.

Parameter	Free space	On body	
Operating frequency (GHz)	3.5	3	3.5
Reflection coefficient (dB)	−16.29	−17.04	−13.8
Bandwidth (MHz)	2306	1461	
Peak gain (dB)	6	−5.3	−7.5

Table 2. Comparison of the WST antenna with other flexible antennas available in literature (with λ_g = lower operating wavelength).

Ref.	Size (mm/λ_g)	Operating frequency (GHz)	Bandwidth (%)	Peak gain (dBi)	Substrate material	Flexible?	SAR (W/kg)
[16]	$62 \times 62 \times 5.5$/ $0.83 \times 0.83 \times 0.073$	3.5/5.8	11.7/9.1	6.6/7.2	Felt	Yes	0.128
[17]	$62 \times 62 \times 4$/ $0.83 \times 0.83 \times 0.053$	3.5/5.8	12.5/11.6	6/5.8	Felt	Yes	0.202/0.074
[18]	$70 \times 70 \times 2$/ $0.64 \times 0.64 \times 0.018$	2.38/3.5	4.1/7.0	1.38/7.7	Felt	Yes	Less than 0.72
[19]	$55 \times 55 \times 1.574$/ $0.24 \times 0.24 \times 0.007$	0.99/3.5	4.1/12.5	2.45/7.73	Leather	Yes	0.016/0.695
[20]	$20 \times 18 \times 0.1$/ $0.44 \times 0.4 \times 0.002$	3.55	17.57	2.06	Polyimide	Yes	Not reported
[21]	$27.4 \times 15.6 \times 0.125$/ $0.6 \times 0.34 \times 0.003$	3.5	16.81 (545 MHz)	2.07	Kapton HN	Yes	Not reported
WST antenna	$32 \times 42 \times 3$/ $0.38 \times 0.5 \times 0.036$	3.5	66	6	Felt	Yes	1.11

To ensure that the WST antenna can be used safely on the human body, the antenna is placed on the phantom body's chest to analyze its specific absorption rate (SAR). As shown in Fig. 17, the simulated maximum SARs averaged over 1-g of tissue are 1.11 W/kg at 3 and 3.5 GHz, fulfilling the IEEE C95.1-2005 requirement of 1.6 W/kg.

Table 2 compares the WST antenna with other flexible planar antennas from literature operating in the same frequency range. It can be seen that the proposed antenna shows significantly improved bandwidth and increased compactness, as follows:

a. Its impedance bandwidth is improved compared to antennas proposed in [16–21].
b. Its gain is higher than the antennas in [20, 21], which used polyimide and Kapton HN substrates, respectively.

   Its size is more compact than antennas proposed in [16–19].

6. CONCLUSION

This work proposes an innovative design of a WST antenna for 5G applications. Simulations indicate an impedance bandwidth of 2306 MHz from 3.14 to 5.45 GHz, a peak gain of 6 dB at 3.5 GHz, and a radiation efficiency of more than 87%. Moreover, the proposed antenna is wideband, mechanically flexible, low profile, and robust in performance. The proposed textile antenna shows a low SAR level even when it is placed near the chest of the human body. The experimental results validate that the prototype antenna can be used potentially for wearable applications.

ACKNOWLEDGMENT

This work was funded in part by the Academy of Finland 6G Flagship program (grant no: 318927).

REFERENCES

1. Jovanov, E. and A. Milenkovic, "Body area networks for ubiquitous health-care applications: Opportunities and challenges," *J. Med. Syst.*, Vol. 35, No. 5, 1245–1254, Oct. 2011.
2. Martinez, I., et al., "Compact, low-profile and robust textile antennas with improved bandwidth for easy garment integration," *IEEE Access*, Vol. 8, 77490–77500, 2020, doi: 10.1109/ACCESS.2020.2989260.
3. Mashaghba, H. A., et al., "Bending assessment of dual-band split ring-shaped and bar slotted all-textile antenna for off-body WBAN/WLAN and 5G applications," *2020 2nd International Conference on Broadband Communications, Wireless Sensors and Powering (BCWSP)*, 1–5, 2020, doi: 10.1109/BCWSP50066.2020.9249403.
4. Német, A., S. Alkaraki, Q. H. Abassi, and S. F. Jilani, "A biodegradable textile-based graphene antenna for 5G wearable applications," *2021 IEEE International Symposium on Antennas and Propagation and USNC-URSI Radio Science Meeting (APS/URSI)*, 1583–1584, 2021, doi: 10.1109/APS/URSI47566.2021.9704120.
5. Biçer, M. B. and E. A. Aydin, "Design and fabrication of rectangular microstrip antenna with various flexible substrates," *2021 International Conference on Innovation and Intelligence for Informatics, Computing, and Technologies (3ICT)*, 360–364, 2021, doi: 10.1109/3ICT53449.2021.9581451.
6. Jalil, M. E. B., M. K. Abd Rahim, N. A. Samsuri, N. A. Murad, H. A. Majid, K. Kamardin, and M. A. Abdullah, "Fractal Koch multiband textile antenna performance with bending, wet conditions and on the human body," *Progress In Electromagnetics Research*, Vol. 140, 633–652, 2013.
7. Garbacz, R. and R. Turpin, "A generalized expansion for radiated and scattered fields," *IEEE Transactions on Antennas and Propagation*, Vol. 19, No. 3, 348–358, May 1971, doi: 10.1109/TAP.1971.1139935.
8. Harrington, R. and J. Mautz, "Theory of characteristic modes for conducting bodies," *IEEE Transactions on Antennas and Propagation*, Vol. 19, No. 5, 622–628, Sep. 1971, doi: 10.1109/TAP.1971.1139999.
9. Harrington, R. and J. Mautz, "Computation of characteristic modes for conducting bodies," *IEEE Transactions on Antennas and Propagation*, Vol. 19, No. 5, 629–639, Sep. 1971, doi: 10.1109/TAP.1971.1139990.
10. Bauer, J. E. and P. K. Gentner, "Characteristic mode analysis of a circular polarised rectangular patch antenna," *Proc. 13th Eur. Conf. Antennas Propag. (EuCAP)*, 1–3, Krakow, Poland, Apr. 2019.
11. Elias, B. B. Q., P. J. Soh, A. A. Al-Hadi, and P. Akkaraekthalin, "Gain optimization of low-profile textile antennas using CMA and active mode subtraction method," *IEEE Access*, Vol. 9, 23691–23704, 2021, doi: 10.1109/ACCESS.2021.3056905.
12. Lamsalli, M., A. El Hamichi, M. Boussouis, N. A. Touhami, and T. Elhamadi, "Genetic algorithm optimization for microstrip patch antenna miniaturization," *Progress In Electromagnetics Research Letters*, Vol. 60, 113–120, 2016.
13. Kaschel, H. and C. Ahumada, "Design of rectangular microstrip patch antenna for 2.4 GHz applied a WBAN," *2018 IEEE International Conference on Automation/XXIII Congress of the Chilean Association of Automatic Control (ICA-ACCA)*, 1–6, 2018, doi: 10.1109/ICA-ACCA.2018.8609703.
14. Miralles, E., C. Andreu, M. Cabedo-Fabrés, M. Ferrando-Bataller, and J. F. Monserrat, "UWB on-body slotted patch antennas for in-body communications," *2017 11th European Conference on Antennas and Propagation (EUCAP)*, 167–171, 2017, doi: 10.23919/EuCAP.2017.7928598.

15. Gupta, A., A. Kansal, and P. Chawla, "Design of a compact dual-band antenna for on-/off body communication," *IETE J. Res.*, 1–9, 2020.
16. Yang, H., X. Liu, Y. Fan, and L. Xiong, "Dual-band textile antenna with dual circular polarizations using polarization rotation AMC for off-body communications," *IEEE Transactions on Antennas and Propagation*, 2021, doi: 10.1109/TAP.2021.3138504.
17. Yang, H. and X. Liu, "Screen-printed dual-band and dual-circularly polarized textile antenna for wearable applications," *2021 15th European Conference on Antennas and Propagation (EuCAP)*, 1–4, 2021, doi: 10.23919/EuCAP51087.2021.9411013.
18. Yang, H. and X. Liu, "Wearable dual-band and dual-polarized textile antenna for on- and off-body communications," *IEEE Antennas and Wireless Propagation Letters*, Vol. 19, No. 12, 2324–2328, Dec. 2020, doi: 10.1109/LAWP.2020.3032540.
19. Regina, S. and A. Merline, "Flexible leather substrate dual-band wearable antenna with impact analysis on testing under wet condition for human rescue system," *Textile Research Journal*, Vol. 91, Nos. 17–18, 1927–1942, 2021, doi:10.1177/00405175211006214.
20. Kumar Naik, K. and D. Gopi, "Flexible CPW-fed split-triangular shaped patch antenna for WiMAX applications," *Progress In Electromagnetics Research M*, Vol. 70, 157–166, 2018.
21. Zakir Hossain, A. K. M., N. B. Hassim, S. M. Kayser Azam, Md. S. Islam, and M. K. Hasan, "A planar antenna on flexible substrate for future 5G energy harvesting in Malaysia," *International Journal of Advanced Computer Science and Applications (IJACSA)*, Vol. 11, No. 10, 2020, doi.org/10.14569/IJACSA.2020.0111020.